PASJ: Publ. Astron. Soc. Japan **59**, S721–S726, 2007 November 28

The Structure and Dynamics of the Quiet Corona from Observations with the Extreme Ultraviolet Imaging Spectrometer on Hinode

Kenneth P. DERE
George Mason University, 4400 University Dr., Fairfax VA, 22030, USA
kdere@gmu.edu
George A. DOSCHEK and John T. MARISKA
Code 7670, Space Science Division, Naval Research Laboratory, Washington, DC 20375-5320, USA
Viggo H. HANSTEEN
Institute of Theoretical Astrophysics, PB 1029 Blindern, University of Oslo, 0315 Oslo Norway
Louise K. HARRA
UCL Mullard Space Science Laboratory, Holmbury St Mary, Dorking, Surrey RH5 6NT, UK
Keiichi MATSUZAKI
Institute of Space and Astronautical Science, Japan Aerospace Exploration Agency, 3-1-1 Yoshinodai, Sagamihara, Kanagawa 229-8510
and
Roger J. THOMAS
Solar Physics Laboratory, Code 671, NASA Goddard Space Flight Center, Greenbelt, MD 20771, USA

(Received 2007 June 1; accepted 2007 September 6)

Abstract

The goal of the Hinode mission is to provide an observational basis for understanding the heating and acceleration of coronal plasmas. On 2007 January 20, the Extreme ultraviolet Imaging Spectrometer performed a raster of a quiet region near Sun center. Maps of intensities, velocities, and electron densities derived from these observations are presented and discussed. Intensity maps in He II λ256, formed at 9×10^4 K, show the chromospheric network. Line intensities of Fe X–XIV, formed at temperatures from 1–2×10^6 K, show small-scale bright points and more extended structures. The intensity map of Fe VIII shows a transition between the two temperatures. The coronal lines reveal regions of high outflow velocities on the order of 100 km s^{-1} in a compact region and 12 km s^{-1} in an extended region. The presence of such high velocities in the quiet corona is an entirely new and unexpected result. Electron densities derived from density sensitive line ratios of Fe XII and XIII are typically 3–20×10^8 cm^{-3}. The highest densities are found in bright, compact areas. For the first time, explosive events in the quiet sun have been observed in the extreme-ultraviolet in He II λ256 profiles.

Key words: line: profiles — Sun: corona — Sun: transition region

1. Introduction

The Hinode satellite was launched in 2006 September and carried aloft a scientific payload of 3 instruments to study the solar atmosphere. These instruments consist of the Solar Optical Telescope (SOT) with the Focal Plane Package (FPP), the X-Ray Telescope (XRT), and the Extreme-ultraviolet Imaging Spectrometer (EIS). Scientific observations began in 2006 December. In this paper we present an analysis of EIS observations of the quiet Sun obtained in 2007 January. These observations demonstrate that EIS is operating as expected and that the analysis of future coordinated observations with all three instruments will provide a valuable basis for understanding the properties of the solar atmosphere.

2. Instrumentation, Observations, and Data Reduction

The EIS instrument consists of an off-axis, parabolic-mirror telescope which focuses an image of the Sun onto the slit of a normal-incidence, toroidal-grating spectrometer. Two sets of molybdenum–silicon multilayer coatings have been applied to two halves of the mirror and grating to enhance their reflectivity in two extreme ultraviolet bands, nominally 170–210 Å and 250–290 Å, the short wavelength (SW) and long wavelength (LW) bands, respectively. There is a 16 pixel offset along the slit between the SW and LW CCD. Two aluminum filters are used to reject visible light. Each wavelength band is detected by a CCD detector. Each CCD pixel views an angle of 0.″9984 along the slit and 22.3 mÅ, the equivalent of 26 km s^{-1} in the SW band and 36 km s^{-1} in the LW band, along the dispersion. A slit exchange mechanism allows 4 different slits with widths 1″, 2″, 40″, and 266″ to be selected. The two widest slits are usually referred to as slots. The observations discussed here were all made with the 1″ slit. The EIS instrument has been described in greater detail by Culhane et al. (2007) and Culhane et al. (2006) and Hinode has been described by Kosugi et al. (2007).

The observations that we will discuss were made on 2007 January 20. The EIS slit was rastered over a region of the quiet Sun near Sun center beginning at 6:05 and ending at 8:17 UT. A single raster consisting of 128 1″ steps with an exposure time of 60 s was performed. The CCD data from the central

512 pixels were transmitted for 17 spectral windows. Data reduction started with the use of the 'Level-0' files produced by the standard data production pipeline. A dark, zero-second exposure obtained on the previous day was subtracted from the Level-0 data by matching their cumulative histograms at the 20% level. Hot pixels were identified from files in the SSW SolarSoft distribution. Further, 'warm' pixels were identified from a 100 s dark exposures obtained on the previous day. A warm pixel is defined as one that has a reproducible dark current that can add up to 10 or more DN for a given exposure time.

The slit image is straight but tilted over the extent of the CCD that was readout. The wavelength scale was corrected for the slit tilt. A wavelength scale has been adopted under the assumption that coronal radial velocities are zero when averaged along the slit. An additional complication to the determination of a velocity scale is the variation of the wavelength scale on a time scale that is roughly equal to the orbital period. At this time, this appears to be related to a thermally induced flexure of the spectrograph. Consequently, the wavelength scale must be corrected for each exposure.

Finally, the profiles were fit with single or double Gaussians by means of a Levenberg–Marquardt algorithm. The statistical weights used in the fitting were derived from the quadrature sum of the photon noise and the CCD read noise. Pixels that were identified as hot or warm pixels were given a weight of zero. The preflight absolute intensity calibration was applied to the data. We refer to the integral of the specific intensity over the Gaussian line profile as the intensity. The velocity is the shift of the center of the fitted Gaussian profile from the position of the rest wavelength.

The area covered by the EIS raster is outlined in the Extreme ultraviolet Imaging Telescope (EIT) image shown in figure 1. The EIT Fe XII image was co-aligned to the EIS spectra by means of the EIS Fe XII image. The accuracy of the co-alignment is on the order of 2.″6, the size of an EIT pixel.

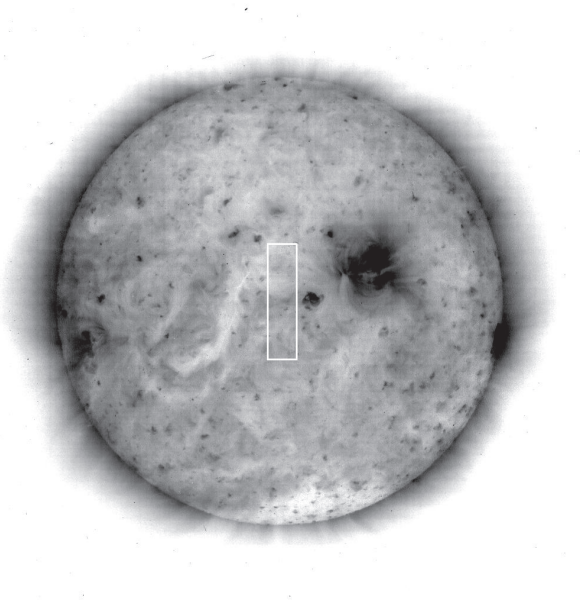

Fig. 1. EIT image in Fe XII λ195 with an outline of the area of the EIS raster.

Table 1. Spectral lines observed.

Ion	Wavelength (Å)	Temperature (K)
He II	256.317	8.9×10^4
Fe VIII	185.213	5.0×10^5
Fe X	184.537	1.0×10^6
Fe XI	188.232, 188.299	1.1×10^6
Fe XII	186.854, 186.887	1.4×10^6
	195.119, 195.179	
Fe XIII	202.044	1.6×10^6
	203.797, 203.828	
Fe XIV	274.204	2.0×10^6
Fe XV	284.163	2.2×10^6

3. Intensities, Velocities, and Densities in the Quiet Sun

In figure 2, spectroheliograms of the quiet Sun in several of the spectral lines observed are shown. The wavelengths and temperatures of peak emissivity are given in table 1. A certain number of artifacts are clearly seen in figure 2 and later in figure 3. First, the Fe XI image, composed of the sum of two Fe XI lines, shows the effect of a dust grain on the CCD detector as a black strip across the lower third of the image. Passage through the South Atlantic Anomaly (SAA) is also seen as two vertical columns on the east and west side of the images. The effect of some, but not all, of the cosmic ray hits has been removed by eliminating pixels where the fit to the line profile was worse than a certain threshold. Finally, not all of the warm pixels have been identified so that their contribution to the line profile could be removed. The chromospheric network is clearly seen in the He II image. The Fe VIII images show the transition from chromospheric structures to coronal structures seen at higher temperature that reveals a combination of small and large-scale structures. Some of the small scale structures can be identified as coronal bright points that connect opposite polarity flux in the MDI images.

A major strength of spectroscopic observations is the ability to determine Doppler shifts from the line profiles and to measure electron densities directly from density-sensitive line pairs. In figure 3 plasma velocities and electron densities derived from lines of Fe XII and Fe XIII are displayed together with the line intensities. The intensities and velocities for Fe XII refer to the strong line at 195.119 Å and for Fe XIII refer to the strong line at 202.044 Å. The Fe XII 195.119 Å line is blended with another Fe XII line at 195.179 Å. However, at the densities measured in the quiet sun (discussed below), the relative intensity of the 195.179 Å line is only about 2% of the stronger line. This is at the level of the noise in most profiles and should not affect the velocities measured in Fe XII. The Fe XII 195 Å line has the greatest signal-to-noise ratio of all of the lines detected in these spectra. Consequently, the velocity patterns are better defined in this line than in any of the others. The correlation of velocities derived from profiles of Fe XII with those derived from Fe XIII indicates that the root-mean-square (RMS) deviation between the two

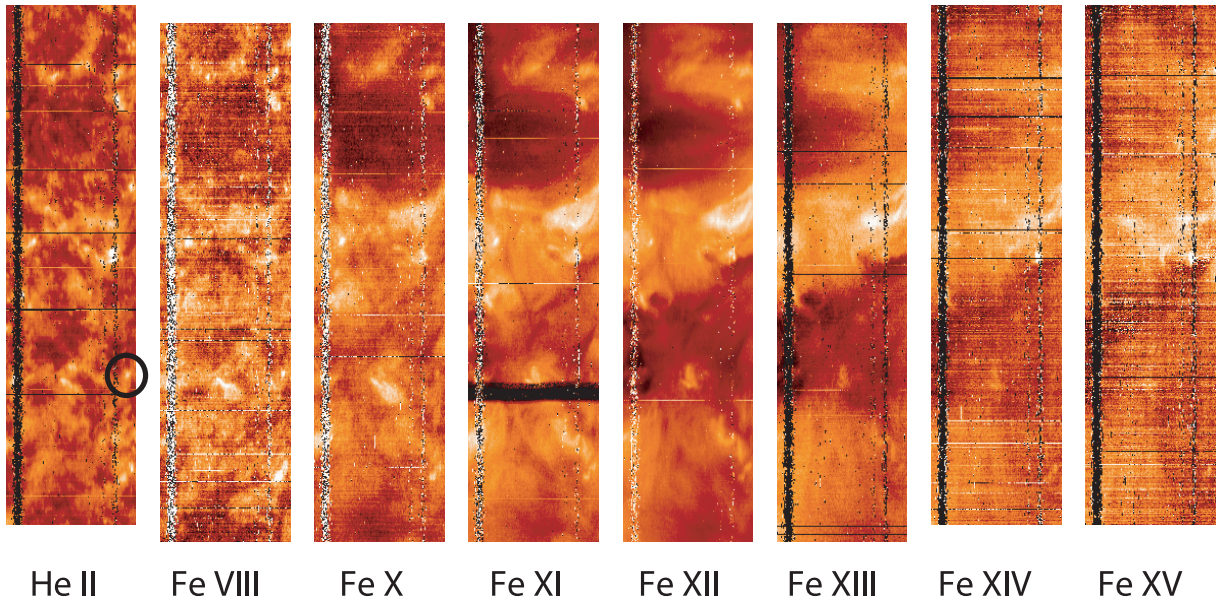

Fig. 2. Spectroheliograms of the quiet Sun over a range of temperatures (see table 1). The circle on the He II image marks the location of the explosive event discussed in section 3.

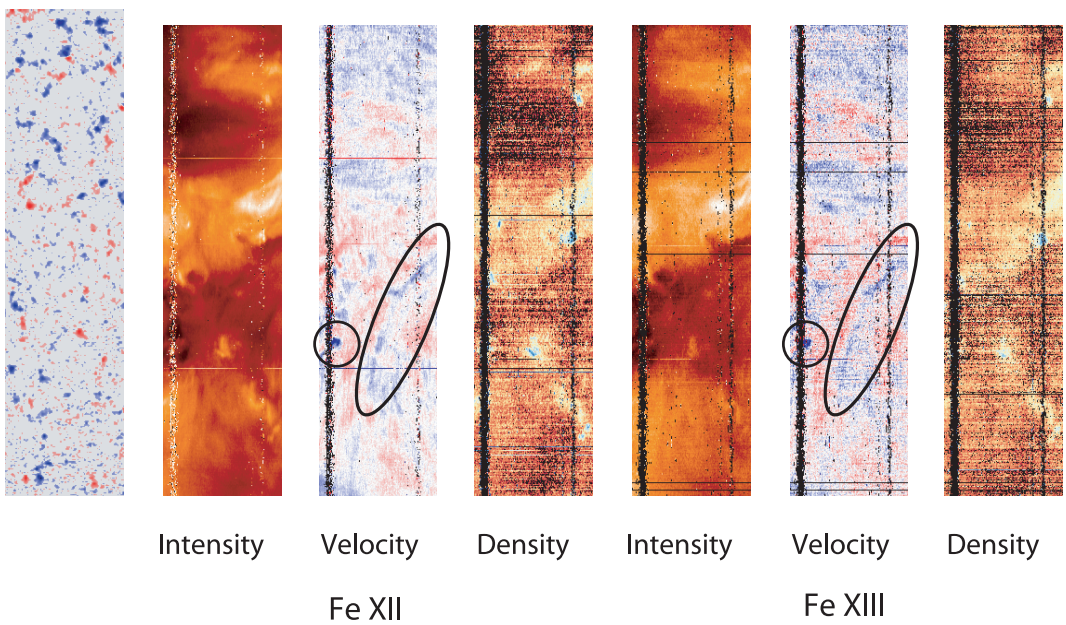

Fig. 3. Intensities, velocities, and densities derived from Fe XII and Fe XIII. The intensities are scaled logarithmically over a factor of 10 in magnitude and the velocities are scaled over a range of $\pm 15\,\mathrm{km\,s^{-1}}$. The densities derived from Fe XII are logarithmically scaled from 2×10^8 (dark) to $2 \times 10^9\,\mathrm{cm^{-3}}$ (blue) and those derived from Fe XIII are logarithmically scaled from 3×10^8 (black) to $3 \times 10^9\,\mathrm{cm^{-3}}$ (blue). Downflows (redshifts) are shown in red, outflows (blueshifts) are shown in blue, zero velocity as white and unreliable data as black. On the far left is the MDI magnetogram of the area observed by EIS.

is $2.3\,\mathrm{km^{-1}}$. If the error where distributed between the Fe XII and the Fe XIII measurements, then the average error in the velocity determination for each line would be $1.6\,\mathrm{km\,s^{-1}}$. Because Fe XII has the better signal-to-noise ratio, it's velocities are somewhat more accurate and those of Fe XIII somewhat less accurate.

It can be clearly seen that the corona is highly structured in its velocity field, something that previous spectroscopic observations had not made apparent. The most notable feature in the velocity images are the high speed outflows that are outlined in black and are apparent in both the Fe XII and Fe XIII images. Spectral line profiles for the area of outflow outlined with a circle are shown in figure 4. The line profile averaged over several pixels in the center of the blueshifted area is plotted as a solid line while nearby profiles are plotted as dashed lines. The red wings of all 3 profiles are very similar

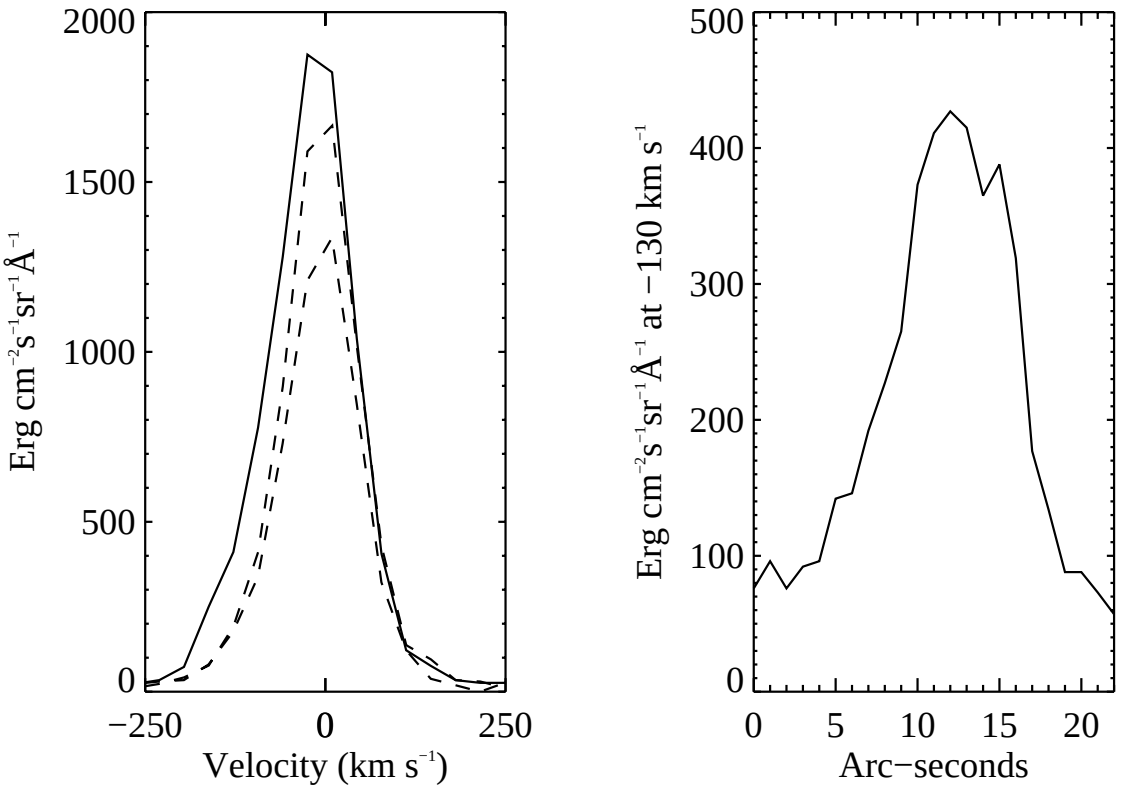

Fig. 4. Left—Fe XII spectral line profiles of the area outlined with a circle in figure 3. The profile at the center of the region of strong blue shifts is indicated by a solid line and the profiles just north and south of this region by dashed lines. Right—The specific intensity in the blue wing of Fe XII as measured along the slit.

and the primary difference is seen in the blue wing. The stigmatic spectra show that the area of outflow is a combination of a low-velocity component and a high-velocity component with outflow velocities ranging from 0 to 200 km s^{-1}. The high-speed outflow appears to be situated on the network boundary as defined by the He II λ256 line. However, it is not possible to identify a similar Doppler signature in the He II velocity map. The profile of the feature in the spatial direction indicates a full-width-at-half-maximum extent of 8″. These large velocities were observed just after the spacecraft left the SAA but their signatures do not appear to be affected by fluxes of high energy particles striking the detector. Further, they are observed in several rasters and in several spectral lines. Consequently, they must be consider real solar phenomena. The extended region of strong outflows, outlined by the ellipse, has a length of about 120″ period Maximum outflow velocities in the area are of the order of 12 km s^{-1}. The coherent outflows along a curvilinear structure are suggestive of a magnetic loop rising out of the solar atmosphere. However, there is no indication of a loop at this position, which is not especially bright, in any of the intensity images. These observations appear to be the first to show the presence of such high speed outflows in the quiet solar corona.

This region was also observed with the XRT instrument on Hinode and with the SECCHI/EUVI instruments on STEREO and we have examined these data sets. The XRT instrument is primarily sensitivity to higher temperatures than seen with EIS and, consequently, the XRT observations show very little in the EIS field-of-view. The SECCHI/EUVI images were taken at a 10 min cadence and show structures similar to those observed with EIS with the small-scale structures showing the greatest evolution with time. There is little evidence in the SECCHI/EUVI to suggest that strong outflows would be found in the areas where they are seen in the EIS spectra.

Electron densities have been determined using calculations of the density sensitivity from the CHIANTI database (Dere et al. 1997; Landi et al. 2006) for the Fe XII λ186/λ195 ratio and for the Fe XIII λ203/λ202 line ratio. As seen in table 1, both Fe XII lines and the Fe XIII line at 203 Å are blends of two lines of the same ion. For Fe XII, the scattering calculation of Storey et al. (2005) is used. This calculation solved the apparent discrepancy between densities obtained from Fe XII line ratios and those from other ions. For Fe XIII the R-matrix calculation of Gupta and Tayal (1998) is used. The most probable Fe XII density is 3×10^8 cm^{-3} and the most probable Fe XIII density is 5×10^8 cm^{-3}. Storey et al. (2005) found quiet sun densities of about 8×10^8 cm^{-3} from the same Fe XII line ratio. Landi and Landini (1998) derived densities of 1.4–1.7 $\times 10^9$ cm^{-3} in the quiet Sun from Fe XIII line ratios. While the Fe XIII densities are typically a factor of 1.6 higher than those obtained from Fe XII, the RMS deviation from this ratio is a factor of 2.2. If attributed equally to errors in the Fe XII and Fe XIII determination, the density measurements in the two lines each have an RMS error of about a factor of 1.6.

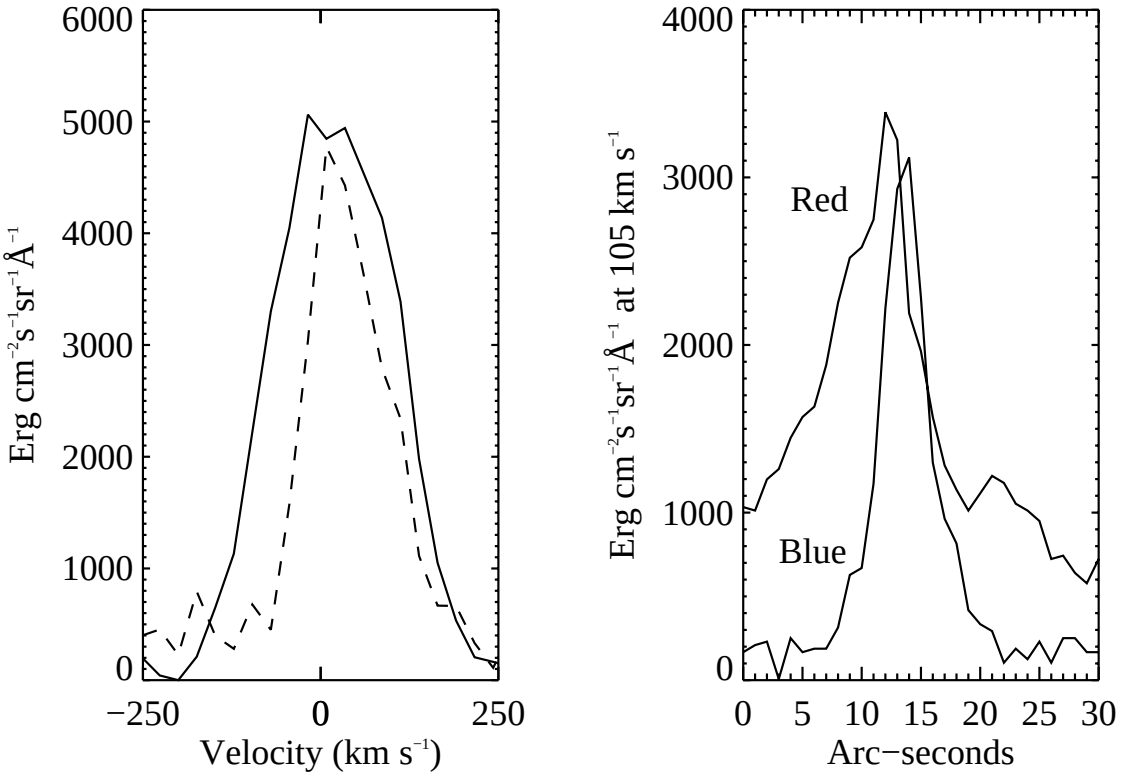

Fig. 5. Left—He II profile of an explosive event (solid line) and a nearby profile (dashed line). Right—intensities of the He II line at $\pm 105\,\mathrm{km\,s^{-1}}$.

This is confirmed by comparing neighboring measurements of the density obtained from Fe XII.

The density maps shown in figure 3 suggest that there is a correlation between density and intensity. Quantitatively, the correlation is very loose. Nevertheless, the densities derived from the two line ratios show a good spatial correlation. The small bright areas in figure 3 have densities on the order of $1\text{–}1.6 \times 10^9\,\mathrm{cm^{-3}}$ with good agreement between the Fe XII and Fe XIII density measurements. The areas with a yellow color in the density maps have densities on the order of $5 \times 10^8\,\mathrm{cm^{-3}}$ as determined from Fe XII and $1 \times 10^9\,\mathrm{cm^{-3}}$ as determined from Fe XIII. The deep orange areas have densities on the order of $2.5 \times 10^8\,\mathrm{cm^{-3}}$ as determined from Fe XII and $5 \times 10^8\,\mathrm{cm^{-3}}$ as determined from Fe XIII.

The MDI magnetogram shown in figure 3 has been visually co-aligned to the EIS observations by comparing it to the intensity maps of He II λ256. The accuracy of the co-alignment is estimated to be on the order of 1″–2″.

The determination of flow velocities in the transition region from the He II 256 Å line are more problematic because of several blends on the long wavelength side of the line. Further, transition region lines such as He II λ256 tend to show a general downflow of about $6\,\mathrm{km\,s^{-1}}$ (Doschek et al. 1976; Dere et al. 1984). At the EIS wavelengths, it is difficult to determine an absolute wavelength scale and, consequently, this issue is not addressed here. Nevertheless, explosive events, first discovered by Brueckner and Bartoe (1983) with the High Resolution Telescope and Spectrograph (HRTS), have been clearly detected. In figure 5, spectral and spatial profiles of an explosive event are shown. The location of the explosive event is marked by the black circle on the He II image seen in figure 2. The spectral line profile extends out to about $100\,\mathrm{km\,s^{-1}}$ in both the red and blue wings and are commensurate with the velocities found in the HRTS data (Dere et al. 1989). The FWHM of the spatial profile in the blue wing is about 3.3×10^3 km (4.″5) which is about twice the size (1.5×10^3 km) found by Dere et al. (1989). The position of the blue wing is slightly offset from the red wing as often found with HRTS. The red wing is also generally more intense along the slit than the red wing due to the blends mentioned previously.

4. Summary

A set of observations of the quiet Sun made with the EIS instrument on Hinode have been analyzed and discussed. A compact region with $100\,\mathrm{km\,s^{-1}}$ outflows has been detected in coronal line profiles in the quiet Sun. In addition, the velocity field of the quiet corona is shown to be highly structured. To our knowledge, these are a completely new results. The electron density has been measured and found to vary with brighter, compact features tending to be about 50% denser than weaker, extended features. Explosive events have been detected in He II λ256. It has been suggested that they are the signature of magnetic reconnection (Dere et al. 1991) and it will be of great interest to explore their relationship to the photospheric field that can be measured with the Solar Optical Telescope on Hinode.

Hinode is a Japanese mission developed and launched by ISAS/JAXA, with NAOJ as domestic partner and NASA and STFC (UK) as international partners. It is operated by these agencies in co-operation with ESA and NSC (Norway). We are grateful for the use of MDI and EIT data obtained on the SOHO spacecraft. SOHO is a project of international cooperation between ESA and NASA. This research has made use of NASA's Astrophysics Data System.

References

Brueckner, G. E., & Bartoe, J.-D. F. 1983, ApJ, 272, 329
Culhane, J. L., et al. 2007, Sol. Phys., 243, 19
Culhane, J. L., et al. 2006, Proc. SPIE, 6266, 62660T
Dere, K. P., Bartoe, J.-D. F., & Brueckner, G. E. 1984, ApJ, 281, 870
Dere, K. P., Bartoe, J.-D. F., & Brueckner, G. E. 1989, Sol. Phys., 123, 41
Dere, K. P., Bartoe, J.-D. F., Brueckner, G. E., Ewing, J., & Lund, P. 1991, J. Geophys. Res., 96, 9399
Dere, K. P., Landi, E., Mason, H. E., Monsignori Fossi, B. C., & Young, P. R. 1997, A&AS, 125, 149
Doschek, G. A., Feldman, U., & Bohlin, J. D. 1976, ApJ, 205, L177
Gupta, G. P., & Tayal, S. S. 1998, ApJ, 506, 464
Kosugi, T., et al. 2007, Sol. Phys., 243, 3
Landi, E., Del Zanna, G., Young, P. R., Dere, K. P., Mason, H. E., & Landini, M. 2006, ApJS, 162, 261
Landi, E., & Landini, M. 1998, A&A, 340, 265
Storey, P. J., Del Zanna, G., Mason, H. E., & Zeippen, C. J. 2005, A&A, 433, 717